JOURNAL OF GEOPHYSICAL RESEARCH, VOL. 112, D08201, doi:10.1029/2006JD007899, 2007

Effects of ice crystal habit on thermal infrared radiative properties and forcing of cirrus

Manfred Wendisch,[1,2] Ping Yang,[3] and Peter Pilewskie[4]

Received 10 August 2006; revised 16 October 2006; accepted 9 November 2006; published 17 April 2007.

[1] The impact of assumed ice crystal morphology on thermal infrared (IR) radiative properties of subtropical cirrus is quantified. In particular, the crystal-shape-dependent profiles of downwelling and upwelling thermal IR (broadband and spectral) irradiances and the radiative forcing of cirrus (at the top and bottom of the atmosphere) are investigated. For this purpose, airborne measurements of ice crystal size distribution (in terms of ice crystal maximum dimension) from the CRYSTAL-FACE campaign and a recently published library of thermal IR optical properties of nonspherical ice crystal habits are implemented into radiative transfer simulations. Two cirrus cases are studied in detail: (1) a high (cold) cirrus with small optical thickness ($\approx$1 at 10.8 μm wavelength) and (2) a lower (warmer) cirrus of relatively large optical thickness ($\approx$7). The relative effects of ice crystal shape on thermal IR irradiance are substantial for the high, optically thin cirrus (up to 70%). Spectrally, the largest effects of ice crystal shape are identified in the atmospheric window spanning from 8 to 12 μm wavelengths, especially for the upwelling irradiance above the cirrus. For the low cirrus of large optical thickness the thermal IR irradiance is only slightly sensitive to ice crystal habit (less than 15–20%). Within the major gas absorption bands the thermal IR radiation is essentially insensitive to ice crystal shape. Furthermore, it is concluded that the thermal IR radiative forcing at the top of the atmosphere contains significant ice crystal shape dependence for the high cirrus case.

Citation: Wendisch, M., P. Yang, and P. Pilewskie (2007), Effects of ice crystal habit on thermal infrared radiative properties and forcing of cirrus, *J. Geophys. Res.*, *112*, D08201, doi:10.1029/2006JD007899.

1. Introduction

[2] Cirrus clouds are widespread over the globe and constitute an essential component of the Earth's climate system [*Lynch et al.*, 2002]. They scatter and absorb solar radiation (wavelengths between 0.3 and 4 μm), and absorb and emit radiation in the thermal infrared (IR) spectral range (about 4–100 μm, also called terrestrial or longwave spectral range). In this way cirrus clouds influence the radiative energy budget of the Earth.

[3] Thin and high (cold) cirrus clouds warm the atmosphere in a manner similar to IR active (greenhouse) gases such as H_2O or CO_2 [e.g., *Liou*, 1986]. Longwave radiation emitted by the lower (warmer) atmosphere and the surface is absorbed by these clouds. However, because the cirrus is situated in high altitudes, i.e., colder atmospheric environments, the cirrus clouds emit at much lower temperatures. Therefore the IR emission to space is lower in their presence. Some of the emitted radiation is directed downward thus adding to the net (solar plus longwave) radiation at the surface and lower atmosphere. However, as pointed out by, e.g., *Baran* [2004], the combined solar and thermal IR radiative effect of cirrus may also be cooling, depending on the vertical position (temperature) of the cirrus, its optical thickness and microphysical properties. Optically thick and low (warm) cirrus may cool the atmosphere if the solar albedo effect (reflection of solar energy back to space) exceeds the longwave warming.

[4] Ice crystal shape and size distribution may have a significant impact on the sign (warming or cooling) of the radiative forcing of cirrus clouds [*Zhang et al.*, 1999]. Also there are effects of crystal shape on the remote sensing of cirrus microphysical and optical properties from thermal IR radiation measurements [e.g., *Stubenrauch et al.*, 1999; *Baran et al.*, 1999; *Rädel et al.*, 2003]. In this context also the paper by *Mitchell et al.* [1996] has to be mentioned. This study of *Mitchell et al.* [1996] described the sensitivity of cirrus emissivity at constant Ice Water Content (*IWC*) to crystal shape over the wavelength range 4–175 microns (similar to the current paper, but *Mitchell et al.* [1996] did not address irradiances).

[5] To investigate the net (i.e., combined solar and thermal IR) radiative impact of cirrus, radiative transfer simulations are required which are often based on micro-

[1]Leibniz-Institute for Tropospheric Research, Leipzig, Germany.
[2]Now at Institute for Atmospheric Physics, Johannes Gutenberg-University, Mainz, Germany.
[3]Department of Atmospheric Sciences, Texas A&M University, College Station, Texas, USA.
[4]Laboratory for Atmospheric and Space Physics, Program in Atmospheric and Oceanic Science, University of Colorado, Boulder, Colorado, USA.

0148-0227/07/2006JD007899$09.00

physical measurements and the optical properties (scattering and absorption) of the individual ice crystals of the cirrus cloud. These optical quantities depend on the size and shape of the ice crystals, as well as on the wavelength of the incident radiation. The size of ice crystals in cirrus covers a broad range (from micrometers to millimeters). For the simulations of cirrus net radiative forcing a wavelength range from the near ultraviolet (UV) to the far IR (0.3–100 μm) has to be covered. Because cirrus clouds are most prevalent at high altitudes (cold environments), these clouds mainly consist of nonspherical ice crystals with complicated scattering and absorption features. Elaborate numerical techniques are required for computing the optical properties of the individual nonspherical ice crystals. Although these methods are established [*Mishchenko et al.*, 2000], there is no single tool which concurrently covers all feasible ice crystal sizes, wavelengths (near UV to far IR) and ice crystal shapes [*Fu et al.*, 1999].

[6] Until recently most of the studies on the radiative impact of nonspherical ice crystal habit have focused on the solar part of the spectrum [see, e.g., *Mitchell and Arnott*, 1994; *Macke et al.*, 1998; *McFarquhar et al.*, 2002; *Schlimme et al.*, 2005; *Wendisch et al.*, 2005, and numerous references therein]. For the thermal IR spectral range similar systematic investigations to evaluate the influence of differently shaped ice crystals on thermal IR cirrus radiative properties are fewer [e.g., *Francis et al.*, 1999; *Yang et al.*, 2001; *Baran and Francis*, 2004; *Baran*, 2005]. This is partly due to the lack of affordable (in terms of computer requirements) numerical tools to calculate the scattering and absorption properties of nonspherical ice crystals in the thermal IR wavelength range.

[7] At present, there is no specific method that can be applied to the computation of the optical properties of nonspherical particles with sizes spanning from Rayleigh scattering regime (particle size much smaller than wavelength of incident radiation) to the geometric optical regime (particle size much larger than wavelength). Recently, using a combination of several light scattering computational methods on the basis of the approach suggested by *Fu et al.* [1998], *Yang et al.* [2005] calculated the optical properties for ice crystals (seven different shapes were assumed) with maximum dimensions from about 2 to 9,500 μm within the wavelength range from 3 to 100 μm. *Yang et al.* [2005] provided their results in the form of look-up tables.

[8] In this paper we have used this library of optical properties (for thermal IR wavelengths) of individual, nonspherical ice crystals by *Yang et al.* [2005] to study the impact of ice crystal habit on the thermal IR (broadband and spectral) radiative transfer through cirrus. Instead of using parameterized ice crystal size distributions as done by, e.g., *McFarquhar and Heymsfield* [1997], we have utilized specific in situ measurements of two cirrus clouds from a field campaign. These were the same microphysical measurements (ice crystal size distributions) as used by *Wendisch et al.* [2005, hereafter referred to as W05]. In this way the present paper is a companion to W05.

[9] In W05 the effects of ice crystal morphology on solar spectral irradiance and cirrus forcing were investigated in detail. In situ measurements of ice crystal size distribution were used in W05 to calculate profiles of solar spectral irradiance above and below the cirrus and its solar radiative forcing. Spheres and nonspherical ice crystal habits (columns, hollows, plates, bullets, and aggregates) were assumed in the simulations. Two cirrus cases (optically thin cirrus and cirrus of moderate optical thickness) were investigated in W05. The second case had an optical thickness of about 7, which is considered "moderate" in the solar spectral range. However, in the thermal IR such an optical thickness is large; the emission of such a cloud is nearly identical to 1 and thus the cloud is "black" in the thermal IR. Therefore this second cirrus case is called "cirrus of large optical thickness" in the following text, although the same case is called "moderately optically thick" in W05.

[10] The major conclusion of W05 was that the impact of shape characteristics of the ice crystals is important for the reflected irradiance above the optically thin cirrus, especially for small solar zenith angles. In this situation single-scattering dominates the reflected solar radiation and thus angular details of the nonspherical phase function persist in the cirrus scattered radiation field. For the cirrus of large optical thickness (when multiple scattering is important) the effects of ice crystal habit were found to be of minor importance because of the integrative influence of many successive scattering events.

[11] This paper is divided into the following sections. In section 2 the measured data (microphysical and radiation) utilized here are briefly introduced. Section 3 elucidates how the microphysical measurements and the optical library of *Yang et al.* [2005] are combined and used to drive the radiative transfer model and to simulate profiles of downwelling and upwelling thermal IR irradiance. In the primary section of this paper, section 4, the impact of ice crystal shape on thermal IR irradiance (broadband and spectral) and radiative forcing of the cirrus (at top and bottom of the atmosphere) are simulated and discussed. Section 4 also compares calculated broadband thermal IR irradiances with coincident measurements. A summary and the major conclusions are presented in section 5.

2. Experimental Section

[12] Airborne measurements of profiles of ice crystal number size distribution (as a function of maximum dimension of the crystals), meteorological (drop sounding measurements of profiles of air temperature, pressure, and relative humidity), and thermal IR radiation measurements were conducted during the Cirrus Regional Study of Tropical Anvils and Cirrus Layers–Florida Area Cirrus Experiment (CRYSTAL-FACE) [*Jenson et al.*, 2004]. Data from CRYSTAL-FACE are used in this study. The measurements used here were collected by three aircraft. The microphysical, in situ size distribution data were taken by the National Aeronautics and Space Administration (NASA) WB-57F aircraft. A second NASA aircraft (ER-2) performed broadband thermal IR irradiance measurements above the cirrus. The Naval Research Laboratory CIRPAS (Center for Interdisciplinary Remotely Piloted Aircraft Studies) Twin-Otter (type UV-18A) aircraft sampled broadband thermal IR irradiance data below the cirrus.

[13] The broadband upwelling and downwelling thermal IR irradiance measurements were obtained using CG-4 pyrgeometers (manufactured by Kipp & Zonen, Delft, The

Table 1. Ice Crystal Habits Included in This Study[a]

Ice Crystal Shape	Curve Notation
Sphere	thick solid lines
Droxtal	long dashes
Solid hexagonal column	dotted lines
Hollow hexagonal column	dash-dot-dot-dotted lines
Hexagonal plate	dash-dotted lines
Bullet rosette	dashed lines
Aggregate	thin solid lines

[a]The curve notation is applied in all figures of this paper.

Netherlands) mounted on the ER-2 and Twin-Otter. These pyrgeometers are sensitive to thermal IR radiation in the wavelength range from 4.5 to 42 μm. The microphysical measurements were collected from a suite of instruments on board the WB-57 which were discussed in detail in W05.

[14] Two specific cirrus clouds (the same as in W05) are analyzed in this paper. On 26 July 2002 an optically thin, high (cold) cirrus was sampled at altitudes between 13.1 and 15.4 km. The ER-2, equipped with the CG-4 pyrgeometers, was flying above this cirrus, while the microphysical properties were measured within the cirrus from instruments on board the WB-57. For this cirrus case no concurrent pyrgeometer measurements by the Twin-Otter below the cirrus were available. The second cirrus case investigated here was observed on 23 July 2002. On that day a cirrus of larger optical thickness was sampled between 6.4 and 8.0 km altitude by the radiation and microphysical instruments mounted on the three aircraft. An overview of the general characteristics of the two clouds is given in Table 1 of W05.

[15] The aircraft flight patterns for these two cirrus cases were identical to those selected in W05 (see Figures 1 and 3 in W05). The original selection of these patterns was performed in W05 after careful screening of the entire CRYSTAL-FACE data set. The three criteria for the selection of the cases were (1) available profile measurements of the microphysical properties through the cirrus measured by the WB-57F; (2) available irradiance data above the cirrus collected by the ER-2, and if possible, by the Twin-Otter below cirrus; and (3) close vertical colocation (in space and time) between the two radiation aircraft (ER-2 and Twin-Otter) and the microphysical measurements conducted by the WB-57F. The final time periods of the flight paths were then chosen in W05 after inspection of the reflected solar spectral irradiance measured by the downward looking part of the NASA Solar Spectral Flux Radiometer (SSFR) mounted at the ER-2, which had to be sufficiently constant along the flight path. For compatibility reasons we use the same selected flight paths from W05 in this paper.

3. Radiative Transfer Simulations

[16] A similar modeling strategy as described in W05 is followed in this paper. However, for the spectral optical properties of individual ice crystals of different sizes in the thermal IR spectral range the look-up tables by *Yang et al.* [2005] are employed here. This database includes the extinction and absorption efficiency, the single-scattering albedo, and the asymmetry parameter of individual nonspherical ice crystals for six crystal habits (see Table 1). The data are given as a function of 45 sizes (corresponding to the size bins of the number size distribution instruments) ranging from 2 to 9,500 μm. These sizes represent the maximum dimensions of the respective crystals. A wavelength range of 3–100 μm is covered by the look-up tables. The effects of ice crystal shape on the optical properties of the individual crystals are discussed in detail by *Yang et al.* [2005].

[17] The optical properties of individual ice crystals are weighted with the corresponding ice crystal number size distribution (measured by the WB-57 as a function of height) in the same manner as described in W05 (see equations (1)–(3) in W05). The resulting profiles of the volumetric spectral optical properties (extinction coefficient, single-scattering albedo, asymmetry parameter) of the ice crystal populations are used as input to the radiative transfer tool libRadtran (library for Radiative transfer) by *Mayer and Kylling* [2005]. The same meteorological input (from drop sondes) and spectral surface albedo as described in W05 was used here to run libRadtran. The discrete ordinate solver DISORT version 2.0 by *Stamnes et al.* [1988] with six streams was applied. The model calculates profiles of spectral upwelling and downwelling irradiance, $F^{\uparrow}_{\lambda}$ and $F^{\downarrow}_{\lambda}$ (in W m^{-2} μm^{-1}), as well as upwelling and downwelling broadband thermal IR irradiance $F^{\uparrow}$ and $F^{\downarrow}$ (in W m^{-2}). The simulations cover the wavelength range from 3.8 to 70 μm. For the broadband simulations the correlated *k*-distribution band parameterization suggested by *Fu and Liou* [1992] was used. For the spectral calculations the SBDART radiative transfer model by *Ricchiazzi et al.* [1998] was applied.

4. Influence of Cirrus Crystal Habit

4.1. Procedure and Scenarios

[18] An overview of the combined measurement-modeling procedure as described in sections 2 and 3 is illustrated in Figure 1. On the basis of the microphysical measurements of the ice crystal size distribution and using the optical library by *Yang et al.* [2005] the volumetric scattering and absorption properties of the ice crystal population are simulated (using equations (1)–(3) in W05). Then radiative transfer calculations are performed as described in section 3. The resulting downwelling and upwelling, thermal IR irradiances (broadband and spectral)

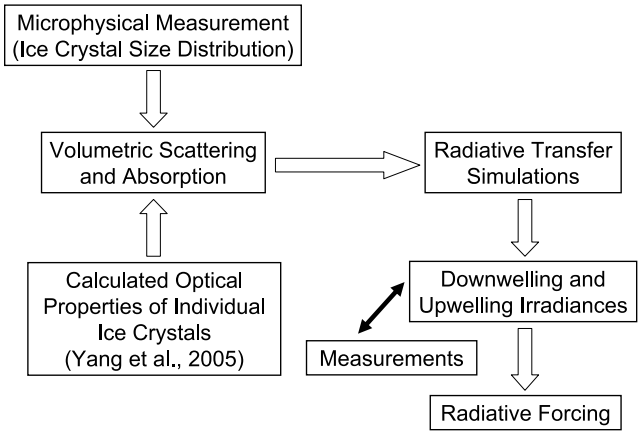

Figure 1. Overview of the methodology combining measurements and simulations.

Table 2. Spectral Optical Thickness (Dimensionless) for Two Cirrus Types (26 July 2002, Optically Thin Cirrus, and 23 July 2002, Cirrus of Large Optical Thickness) and Two Scenarios (N = Constant and IWC = Constant) Assuming Different Ice Crystal Shapes[a]

	26 July 2002: Optically Thin Cirrus		23 July 2002: Large Optical Thickness	
Scenario (Constant =)	N	IWC	N	IWC
Sphere	1.5	1.5	7.1	7.1
Droxtal	1.4	1.7	6.8	7.7
Solid hexagonal column	1.3	2.2	6.0	16.7
Hollow hexagonal column	1.1	2.3	5.0	17.4
Hexagonal plate	0.91	3.5	4.1	20.0
Bullet rosette	0.74	4.5	2.8	24.9
Aggregate	0.57	3.6	1.5	12.4

[a]Wavelength is $\lambda = 10.8$ μm.

are compared to available measurements (pyrgeometer, see section 2) and finally the radiative forcing of the cirrus is derived (see section 4.5).

[19] All simulations in Figure 1 are carried out assuming different ice crystal shapes (see Table 1). Six nonspherical ice crystal habits (droxtals, solid and hollow hexagonal columns, hexagonal plates, bullet rosettes, and aggregates) from the optical library of *Yang et al.* [2005] are considered here. All nonspherical ice particles are assumed to be randomly oriented in space. The detailed geometry of the crystal habits is described by *Yang et al.* [2005, and references therein]. For comparison, we also include ice spheres in the computations.

[20] Two scenarios are investigated in this paper. In the first scenario the number size distribution of the ice crystals as a function of their maximum dimension is conserved. In this way the crystal number concentration N is fixed whereas the Ice Water Content (IWC) varies with crystal shape in the simulations of Figure 1. Spheres have the largest IWC for a given maximum dimension, while aggregates exhibit the lowest IWC in this approach. The purpose of this first scenario is to test the magnitude of shape-related effects on the simulations of cirrus radiative properties when using number size distribution measurements without any additional shape information in the calculations. Usually the maximum size of the individual crystals is measured, but no shape information for each individual crystal is available. If these measured number size distributions of the ice crystals are used in radiative transfer simulations the question arises how the unknown shape information impacts the simulated radiative properties of the cirrus. This scenario addresses this rather instrumental issue.

[21] In the second scenario the IWC is kept constant when varying the crystal habit in the calculations of Figure 1. This was realized by the following procedure: First we have calculated the IWC of the particle size population assuming spherical crystal shapes using the given volume of the individual ice spheres, the number size distribution and an ice density of 0.92 g cm^{-3}. For the nonspherical ice crystal population we have applied the same technique to simulate the IWC. The ratio between the two IWCs (spherical/nonspherical) was used to scale the number size distribution of the ice crystals, such that the resulting IWC is independent of crystal shape. The scaled number size distribution was used subsequently to calculate the volumetric optical properties. In this way the IWC stays constant and is independent of crystal habit. However, as a consequence, N is changing for the different crystal habits, whereas the shape of the number size distribution is retained in this second scenario. This comprises a more physical approach. If, for any reason, the crystal shape varies in the cirrus, then it is realistic that the IWC does not change during this transition. This assumption links N with crystal shape. In fact, extinction and absorption in ice clouds depend on the mass and the total projected cross-sectional area of the crystals but not on N [e.g., *Mitchell et al.*, 1996]. Thus, from the modeling point of view it is more reasonable to keep the IWC constant.

[22] The two scenarios cover most of the options possible in reality and should be considered as extreme cases. As an additional approach we have kept constant the cirrus optical thickness, which revealed a very minor shape sensitivity. This is hardly surprising. If the optical thickness is fixed, then the only parameter carrying shape sensitivity into the radiation calculations is the asymmetry parameter, which is not particularly sensitive to crystal habit in the thermal IR wavelength range.

[23] In the following tables and figures the first scenario is labeled by N (or N = constant) and the second scenario is marked by IWC (or IWC = constant), respectively.

4.2. Cirrus Optical Thickness

[24] The impact of the ice crystal habit on the spectral optical thickness (integral over height of the volumetric extinction coefficient) is quantified in Table 2. The cirrus optical thickness for the two cirrus cases and for the two scenarios (N and IWC scenario) for the exemplarily wavelength of $\lambda = 10.8$ μm is presented in Table 2.

[25] The shape of the ice crystals exerts significant effects on cirrus optical thickness in both cirrus cases studied in this paper. For the first scenario (N = constant) spheres clearly exhibit the largest cirrus optical thickness corresponding to the maximum values of the spectral volumetric extinction coefficient for spheres compared to other ice crystal shapes. This is caused by the largest total projected cross-sectional area characteristic for spheres compared to all other crystal geometries. At the other extreme, aggregates reveal the lowest total projected cross-sectional area and therefore yield the lowest optical thickness in the thermal IR spectral range. This is in agreement with the findings of W05 (for the same scenario) for the solar optical thickness of the cirrus.

[26] For the optically thin cirrus observed on 26 July 2002 the spectral optical thickness at $\lambda = 10.8$ μm ranges between 1.5 (spheres) and 0.57 (aggregates). For the cirrus of large optical thickness of 23 July 2002 the respective range is 7.1 (spheres) to 1.5 (aggregates). This wide range shows that the uncertainties of the optical thickness of the cirrus caused by the shape assumptions may be considerable, when the cirrus optical thickness is derived from measurements of crystal number size distribution without any accompanying shape information.

[27] If the IWC is fixed during the calculations (second scenario), then spheres reveal the lowest, bullet rosettes and aggregates the largest cirrus optical thickness. This holds for

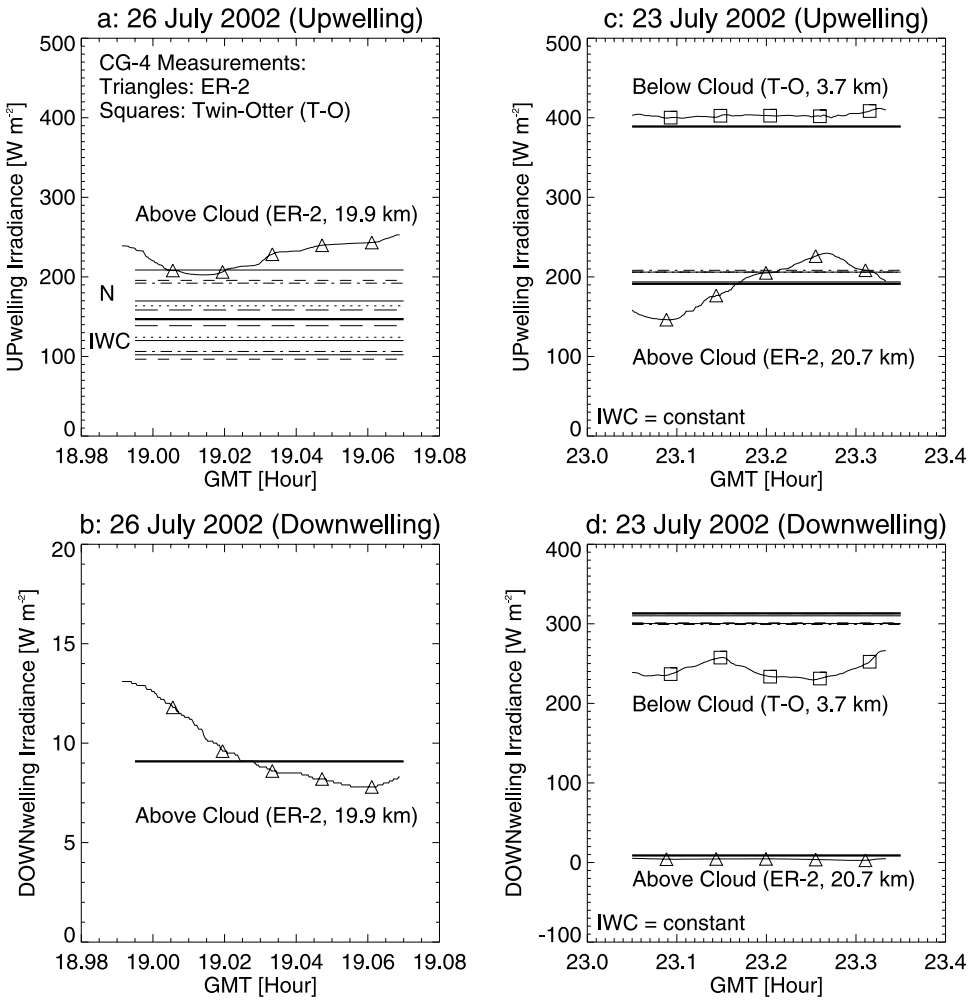

Figure 2. Measured (thin solid lines with open symbols) and simulated (horizontal lines without symbols) broadband thermal IR irradiance for (a and b) the high (cold) optically thin cirrus (26 July 2002) and (c and d) the low (warm) cirrus of large optical thickness (23 July 2002). Open triangles mark the ER-2 pyrgeometer data, and open squares mark the Twin-Otter measurements. The first scenario is labeled by *N* (or *N* = constant), and the second scenario is marked by *IWC* (or *IWC* = constant), respectively. For curve notation, see Table 1.

both cirrus cases investigated here. This opposite behavior compared to the first scenario is again explained by the total projected cross-sectional area, which is decisive for the radiative properties of cirrus in the thermal IR spectral range. In contrast to the first scenario, in the second approach spheres exhibit the smallest total projected cross-sectional area, whereas bullet rosettes and aggregates have a much higher total projected cross-sectional area. The variability of the calculated cirrus optical thickness is similarly large (optically thin cirrus: 1.5 [spheres] to 4.5 [bullet rosettes]; cirrus of large optical thickness: 7.1 [spheres] to 24.9 [bullet rosettes]) compared to the first scenario. This suggests that also in this second scenario crystal habit seriously matters in terms of cirrus optical thickness.

[28] Because the cirrus optical thickness is a major input parameter to the atmospheric radiative models describing the transfer of thermal IR radiation through cirrus, respective shape-related consequences for the thermal IR irradiance and the derived thermal IR radiative forcing of the cirrus can be expected. These will be quantified in the subsequent sections.

4.3. Measured and Simulated Broadband Thermal IR Irradiance

4.3.1. Horizontal Flight Legs

[29] The measured time series of the broadband thermal IR irradiance collected by the CG-4 pyrgeometers along the flight track of the ER-2 and Twin-Otter aircraft are shown in Figure 2 (thin solid lines with open symbols), together with the respective simulations assuming different ice crystal habits (horizontal lines with no symbols). The resulting curve families corresponding to the two scenarios are denoted by *N* and *IWC* respectively. For the optically thin cirrus (26 July 2002) located higher up (13.1–15.4 km) in the atmosphere the curve families of both scenarios are plotted (*N* = constant; *IWC* = constant). For the cirrus of large optical thickness (23 July 2002) which was situated lower (6.4–8.0 km) in the atmosphere the shape sensitivity was generally much smaller; therefore only the results of the

second scenario are shown in this cirrus case. This distinction yields for all subsequent figures.

4.3.1.1. Crystal Shape Effects

[30] In general, the largest shape sensitivity (i.e., largest vertical spread of the horizontal lines) at the respective flight altitudes of the two aircraft is revealed for the upwelling irradiance above the high, optically thin cirrus (see Figure 2a). Certainly, the downwelling irradiance above the two clouds does not show any shape dependence (see Figures 2b and 2d). In those cases only the thick solid line indicating the spherical shape assumption is visible in the figure; the other lines are overlaid.

[31] For the optically thin cirrus (Figures 2a and 2b) there is a significant shape dependence of the upwelling irradiances (above cloud) reflected by the cirrus (see Figure 2a). The total range covered by the simulations is 97–208 W m^{-2}. The first scenario (N = constant, curve family above the thick solid curve) reveals the spheres with the least emitted irradiances, corresponding to the highest cirrus optical thickness in this case (see Table 2). Upwelling IR irradiance above cirrus with spherical particles is lowest in the first scenario because they are the optically thickest and have absorbed most of the longwave IR radiation emitted from below. For the second scenario (IWC = constant, curve family below the thick solid line) the effect is opposite: spheres correspond to the lowest optical thickness (see Table 2) and thus more upwelling irradiance emitted from below is transmitted. Bullet rosettes and aggregates have more total projected cross-sectional area than the other crystal types and therefore exert the strongest impact on upwelling irradiance in the thermal IR for the second scenario (IWC = constant). These nonspherical crystals have less mass per unit length and this enhances N for constant IWC, and thus the total projected area of the ice crystal population is enhanced. As noted above, the radiative properties depend on total area cross section and mass but not N.

[32] The downwelling irradiance above the cirrus (see Figure 2b) is not affected at all by the shape assumption for the crystals of the cirrus, which is no surprise. Also the upwelling and downwelling irradiances above and below the cirrus of large optical thickness (23 July 2002, Figures 2c and 2d) are only moderately influenced by the shape assumptions (see Figures 2c and 2d). In this case the emissivity of the cirrus is nearly identical to 1 regardless of ice crystal shape. Furthermore, this cirrus is situated lower in the atmosphere (6.4–8.0 km) in a much warmer environment. Because the temperature difference between cloud and atmosphere-surface below is less, the contrast in cloud emission and atmosphere-surface emission is also less so crystal morphology has less of an impact.

4.3.1.2. Model-Measurement Comparison

[33] The measured upwelling irradiance at the ER-2 flight level (thin solid line with open triangles in Figure 2a) is higher compared to the simulations, whereas the measured downwelling irradiance above the cirrus (Figure 2b) is well represented by the simulations. The model-measurement discrepancy in Figure 2a can partly be explained by the cirrus horizontal inhomogeneity which is not considered in the simulations. *Fu et al.* [2000] find a similar bias in the outgoing longwave radiation (OLR) emitted by cirrus. These authors postulate that the OLR bias is caused by the neglect of horizontal cirrus inhomogeneities and that the OLR bias is most significant for semitransparent cirrus (low optical thickness) which is located in the cold upper troposphere. That is exactly the case for the cirrus of 26 July 2006. The OLR bias reported by *Fu et al.* [2000] is in the range of −14 W m^{-2} for cirrus with a mean optical thickness of 0.8 and a cloud top height of 11 km. Since the cloud top height in the present cirrus case of 26 July 2002 with low optical thickness is even higher (15.4 km), the OLR bias might easily reach more than 20 W m^{-2}.

[34] For the low (warm), optically thicker cirrus observed on 23 July 2002 (see Figure 2c) there is no such OLR bias. In this cirrus case the measured upwelling irradiance above the cirrus is well represented by the simulations, which is in agreement with what would be expected from the paper by *Fu et al.* [2000].

[35] However, for the downwelling irradiance below the optically thick cirrus there is a gap between measurements and calculations (see Figure 2d). A similar model-measurement discrepancy has been reported in W05 for the solar downwelling irradiance below the cirrus. In W05 the measurements of the reflected solar spectral irradiance above the cirrus was mostly well within the range given by the simulations. Significant discrepancies between measurements and simulations were observed for the transmitted solar spectral irradiance below the cirrus, similar to this study. This suggests that the measurements of the solar and thermal IR irradiance in W05 and this paper are coherent and that the problem is in the respective input to the simulations. In W05 poor colocation of the microphysical and radiation measurements was identified as possible cause for the problems in the measurement-calculation comparison of the downwelling solar irradiance below the cirrus on 23 July 2002. Because of flight safety regulations, the microphysical sampling of the cirrus by the WB-57 was performed about half an hour after the two radiation aircraft (ER-2 and Twin-Otter) have left the flight area. Therefore the necessary close colocation of the microphysical and radiation sampling was not guaranteed on this day. Because in this paper the same microphysical data were used as in W05, similar colocation problems appear here for the thermal IR radiation. Nevertheless, aside from this problem with the radiation below the optically thick cirrus, the measured broadband thermal IR radiation is quite well represented by the simulations.

4.3.2. Profiles

[36] In Figure 3 the simulated profiles of the broadband thermal IR irradiance are displayed (different lines represent the results for the assumed crystal shapes, see Table 1). The results for the two different scenarios are marked by N (first scenario: N = constant) and IWC (second scenario: IWC = constant). Furthermore, the cirrus-free simulations are added as open diamonds. In addition, the available, measured data from the CG-4 pyrgeometers are included in Figure 3 as open squares with horizontal bars. These bars indicate the two-sigma standard deviation of the measured irradiance along the flight leg.

4.3.2.1. Upwelling Broadband Thermal IR Irradiance

[37] In general the cirrus decreases the upwelling broadband thermal IR irradiance above its base height, compared to the cloudless atmosphere (greenhouse effect of cirrus, see Figures 3a and 3c). The strength of this decrease depends on

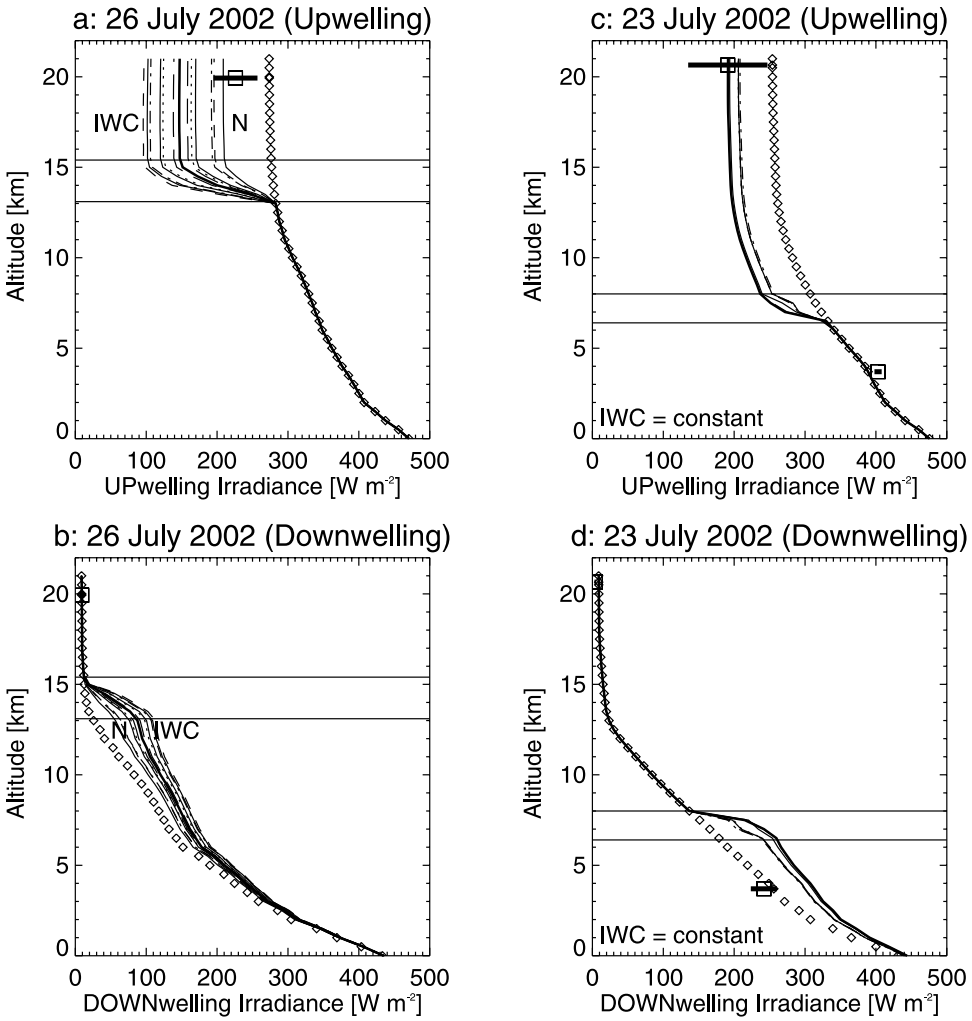

Figure 3. Profiles of simulated broadband thermal IR upwelling and downwelling irradiance. The horizontal lines mark the cirrus top and bottom heights, respectively. The open diamonds indicate the simulations without cirrus (cloudless conditions). The open squares show the average of the respective measured irradiance, with horizontal bars representing the two-sigma standard deviations along the flight track. The first scenario is labeled by *N* (or *N* = constant), and the second scenario is marked by *IWC* (or *IWC* = constant), respectively. For curve notation, see Table 1. (a) Upwelling and (b) downwelling broadband irradiances for the optically thin (high and cold) cirrus observed on 26 July 2002 shown as a function of altitude. (c) Upwelling and (d) downwelling broadband irradiances as a function of altitude for the cirrus of large optical thickness (low and warm) as observed on 23 July 2002.

the altitude of the cirrus (i.e., its temperature) and its optical thickness. The height (temperature) dependence is because the cirrus emits less thermal IR radiation in colder environment (higher altitude). Therefore the higher (colder) the cirrus is situated, the less thermal IR upwelling broadband thermal IR irradiance is emitted by the cirrus, and the larger the difference between the upwelling irradiance under cloudless and cloudy conditions (for constant optical thickness of the cirrus). On the other hand, if the optical thickness of the cirrus is decreased (while its altitude is kept constant), then more thermal IR upwelling radiation from below the cloud penetrates the cirrus and thus its greenhouse effect is smaller. This is true for relatively thin cirrus. Cirrus clouds of optical thickness greater than about 7–10 have emissivity of near unity. Because of the absorption of thermal IR upwelling radiation, the cirrus prevents the transmittance of the relatively higher thermal IR radiation emitted form below which would occur in cloudless conditions (mostly in the atmospheric window wavelength region, 8–12 μm). Thus a lower cirrus optical thickness lessens its greenhouse effect; that is, the difference between upwelling irradiance above the cirrus for cloudy and cloudless conditions is less. Summarizing, a maximum greenhouse effect (i.e., maximum difference between upwelling thermal IR irradiance above the cirrus with and without the cirrus) is expected for high (cold) and optically thick cirrus.

[38] The optically thin cirrus observed on 26 July 2002 was situated at a higher altitude (in colder environment) compared to the cirrus of large optical thickness investigated on 23 July 2002. Therefore the decrease of the upwelling irradiance due to the optically thin cirrus is quite moderate. The competing effects (high altitude but relatively small optical thickness) balance to some degree. The cirrus of large optical thickness (23 July 2002) is situated in lower

(warmer) environment. Again the compensating effects (low altitude but large optical thickness) partly cancel. Therefore the greenhouse effect of both cirrus cases is comparable.

[39] With regard to the crystal shape effects, similar conclusions as in subsection 4.3.1 are drawn (see Figures 3a and 3c). Below the cloud there are no effects of the assumed crystal habit on the upwelling thermal IR irradiances. Above the cloud base there are significant shape-related effects on upwelling irradiance in the cirrus case of small optical thickness (in the range of $\pm 50-60$ W m^{-2} for the two investigated scenarios, see Figure 3a). The shape effects simulated for the two scenarios (N = constant, IWC = constant) are comparable in magnitude, but opposite in sign. Whereas the spherical shape assumption exhibits the strongest greenhouse effect in the first scenario (N = constant), it appears to have the smallest greenhouse impact for the second scenario (IWC = constant). For the cirrus with large optical thickness the impact of crystal shape can be neglected (see Figure 3b).

[40] Furthermore, the OLR bias is clearly visible in the profiles shown in Figure 3a (high, cold cirrus of small optical thickness), whereas no such bias is identified in the case of low (warm) cirrus with large optical thickness (see Figure 3c).

4.3.2.2. Downwelling Broadband Thermal IR Irradiance

[41] In contrast to the upwelling radiation, the cirrus generally increases the downwelling broadband thermal IR irradiance below its top height, compared to the cloudless atmosphere (see Figures 3b and 3d). This is because the cirrus constitutes an additional source of thermal IR radiation which adds to the cloud-free atmosphere emission. Again, the magnitude of this increase depends on the altitude of the cirrus (i.e., its temperature) and its optical thickness. The lower (warmer) the cirrus is located in the atmosphere and the larger the cirrus optical thickness, the stronger is the enhancement of the downwelling thermal IR irradiance below cloud top. Therefore the increase of downwelling broadband thermal IR irradiance beneath the cirrus is larger for the cirrus case observed on 23 July 2002.

[42] It is interesting to note that the cirrus has nearly no impact on the downwelling broadband thermal IR irradiance reaching the surface. The results of the cloudless simulations (open diamonds in all figures) and those taking into account the cirrus converge toward the surface. This is because downwelling irradiance near the surface is dominated by the emission due to water vapor in the lower troposphere. The farther away the thermal IR emission source (in this case the cirrus) is, the less impact it has in terms of thermal IR radiation. Also the shape impact decreases toward the ground.

[43] Consistent with the above discussion, the impact of crystal shape is concluded to be important for the high, optically thin cirrus only. Again the two scenarios (N = constant, IWC = constant) act in contrary direction, as reasoned above.

4.3.2.3. Relative Effects of Crystal Habit

[44] In order to quantify the relative effects of ice crystal habit on broadband thermal IR irradiances, the ratio of the respective irradiances assuming spherical ice crystal habit to those simulated with nonspherical shape assumption is shown in Figure 4. As expected, the relative effects of ice crystal shape are most pronounced for the optically thin cirrus observed on 26 July 2002 (see Figures 4a and 4b). For the upwelling broadband thermal IR irradiance (within and above the cirrus) the relative differences between the simulations assuming spheres and nonspherical calculations are in the range of up to 30% for the first scenario (N = constant) and up to 55% for the second scenario (IWC = constant). For the downwelling broadband thermal IR irradiance (within and below the cirrus) slightly larger relative effects (up to 70% for the first scenario, up to 35% for the second scenario) just below cirrus top are simulated.

[45] For the cirrus of large optical thickness (see Figures 4c and 4d) the relative effects of ice crystal shape are much weaker for both scenarios (only the second scenario with IWC = constant is shown here). The reasons for these shape-related differences between the two cirrus cases are the combined effect of cirrus optical thickness (see Table 2) and height (temperature) of the two clouds. The higher (colder) the cirrus is, the stronger effects of ice crystal shape are visible. For lower (warmer) cirrus the shape impact of the cirrus is partly washed out by the dominating emission of the warm ambient air (water vapor) and thus is less pronounced.

[46] The impact of optical thickness on the strength of the relative effects of ice crystal shape was simulated by artificially varying the optical thickness of the two clouds investigated. This has been done for the first scenario (N = constant). The cirrus volume extinction coefficient profile of 26 July 2002 (optically thin cirrus) was multiplied by a factor of five. As a result the ratios in Figure 4a slightly decreased (from maximum values of 30% to about 25%, not shown here), and those in Figure 4b slightly increased (from maximum values of 70% to about 80%). However, these tendencies were quite small. For the 23 July 2002 case (optically thick cirrus) the cirrus extinction coefficient profile was artificially reduced by dividing the profile values by five. Doing so slightly increased the ratios in Figures 4c and 4d. That means that the cirrus optical thickness is not a dominant factor for the relative effects of ice crystal shape. Instead, it appears that the cirrus altitude regulates most of the effects of ice crystal shape. For high cirrus (which is embedded in a cold environment) the "atmospheric background emission" is small, compared to the emission by the cirrus. Therefore the features due to effects of ice crystal shape (via the optical thickness) become more obvious. If the cirrus is located at lower altitudes, then the gaseous "background" emission by the atmosphere (mainly due to water vapor) dominates over most of the effects of ice crystal shape.

4.4. Spectral Thermal IR Irradiance

4.4.1. High (Cold), Optically Thin Cirrus: 26 July 2002

[47] The spectra of the downwelling (Figures 5a and 5b) and upwelling (Figures 5c and 5d) thermal IR irradiance for the high, optically thin cirrus (26 July 2002) are displayed in Figure 5.

4.4.1.1. Downwelling Spectral Thermal IR Irradiance

[48] At the cirrus top (15.4 km altitude; see Figure 5a) the downwelling thermal IR irradiance is generally small. However, the absorption optical thickness of O_3 (9.6 μm) and CO_2 (15 μm) in the atmospheric layer above the cirrus

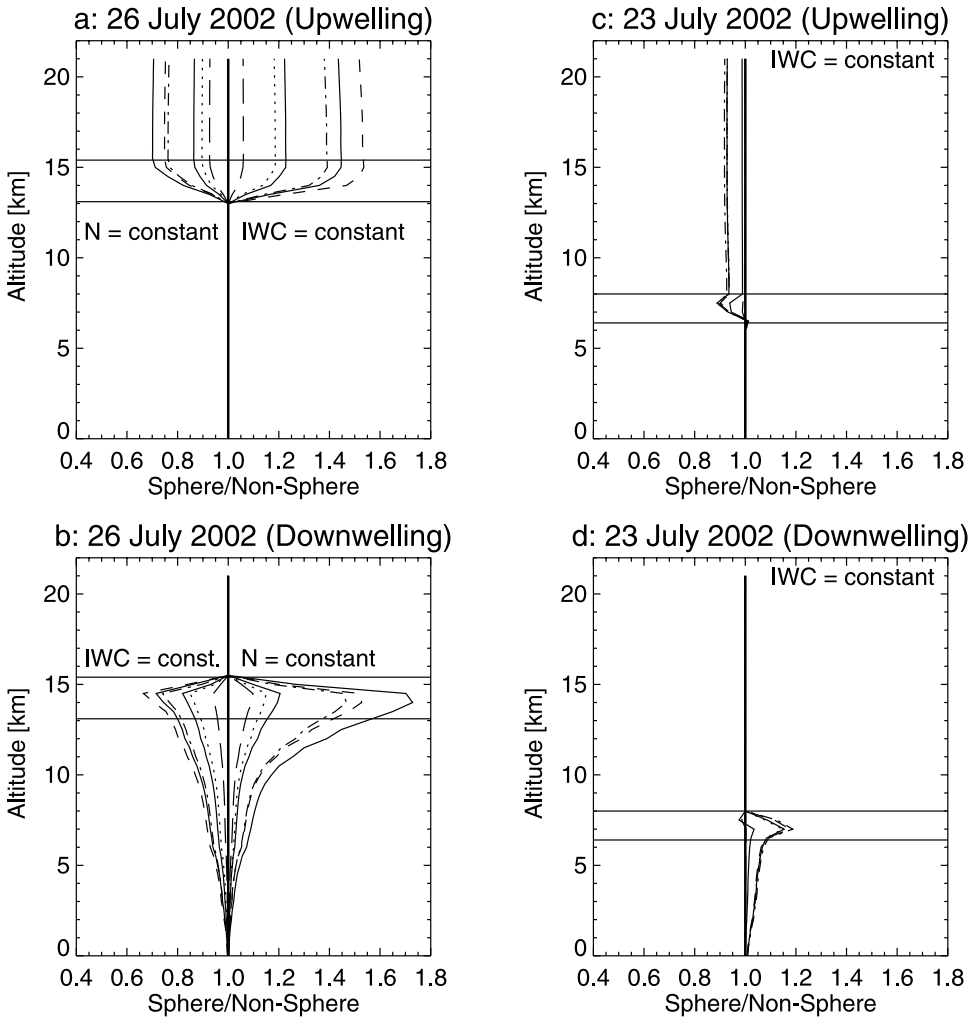

Figure 4. Ratio of broadband thermal IR irradiance, simulated assuming spheres and nonspherical ice crystal shapes. The horizontal lines mark the cirrus top and bottom heights respectively. The first scenario is labeled by *N* (or *N* = constant), and the second scenario is marked by *IWC* (or *IWC* = constant), respectively. For curve notation, see Table 1. Ratio of irradiances simulated assuming spherical and nonsperical crystal shapes for the (a) upwelling and (b) downwelling broadband irradiances as a function of altitude for the optically thin (high and cold) cirrus observed on 26 July 2002. Ratio of irradiances assuming spherical and nonsperical crystal shapes for the (c) upwelling and (d) downwelling broadband irradiances as a function of altitude simulated for the cirrus of large optical thickness (low and warm) as observed on 23 July 2002.

top is sufficiently high so that the thermal IR downwelling radiation roughly corresponds to the respective Planck-emission (asterisks) of the cirrus top layer at the centers of the respective O_3 and CO_2 absorption bands. The emission is quite small because of the low temperatures at this height level. As expected, there are no effects of ice crystal shape at all (for non of the two investigated scenarios) for the downwelling irradiance above the cirrus; all curves (open diamonds for cloudless case, different lines for cirrus cases assuming different ice crystal habits) are not distinguishable from each other.

[49] At the cirrus base (13.1 km, see Figure 5b) the downwelling emitted irradiance increases outside the O_3 and CO_2 absorption bands due to the emission by the cirrus, compared to the cloudless emission (open diamonds) which is not much different from that of Figure 5a. However, the increase in the downwelling irradiance outside the O_3 and CO_2 absorption bands is still moderate because of the low cirrus temperature at this altitude. From these plots deviations from the corresponding blackbody emission spectra (asterisks in Figure 5b) are also obvious. This optically quite thin cirrus cannot be considered a black body (this also means it has an emissivity of less than unity).

[50] Slight effects of ice crystal shape on the downwelling irradiance emitted by the cirrus are obvious in Figure 5b. For the first scenario (*N* = constant) the lines for the different shape assumptions are below the solid thick line (sphere); for the second scenario (*IWC* = constant) the respective lines are above the solid thick line. Assuming the first scenario, if the cirrus consisted of ice spheres only (thick solid line) then it would emit more downwelling radiation compared to the case where it consisted of aggregates (thin solid line). For the second scenario the results are vice versa. This is in correspondence with the

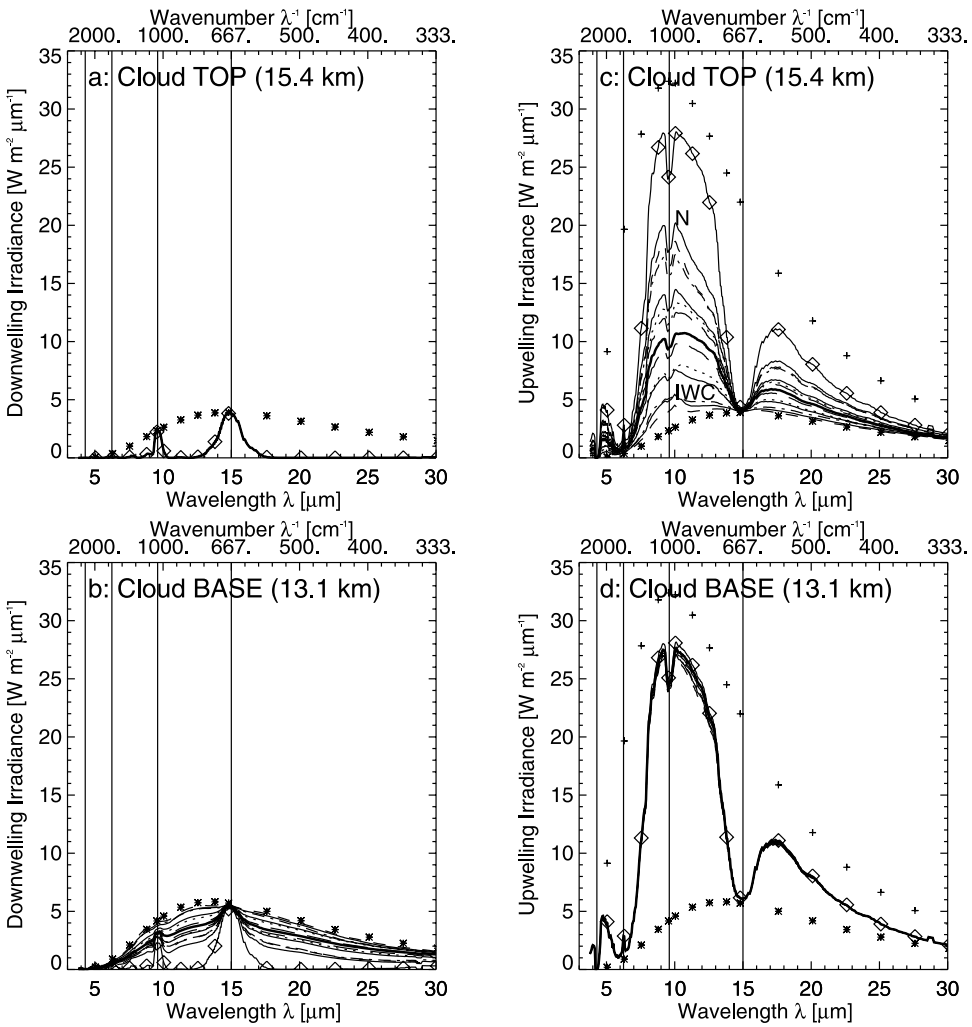

Figure 5. (a and b) Downwelling and (c and d) upwelling spectral thermal IR irradiance at cirrus top (Figures 5a and 5c) and base (Figures 5b and 5d) for the high (cold), optically thin cirrus on 26 July 2002. The vertical lines mark the spectral location of the absorption bands of CO_2 [4.3 and 15 μm], H_2O [6.3 μm], and O_3 [9.6 μm]. Asterisks indicate the blackbody radiation following Planck's law at the respective altitude. The pluses (in Figures 5c and 5d) represent the blackbody radiation emitted by the surface. The open diamonds indicate the simulations without cirrus (cloudless conditions). The first scenario is labeled by *N* (or *N* = constant), and the second scenario is marked by *IWC* (or *IWC* = constant) in Figure 5c. For curve notation, see Table 1.

respective optical thickness of the cirrus (first scenario [second scenario]: cirrus optical thickness largest [smallest] for spheres, smallest [largest] for aggregates, see Table 2).

[51] At the surface (not shown) the downwelling thermal IR spectral irradiance is mainly determined by the emission due to water vapor of the atmosphere beneath the cirrus, essentially the portion near the surface with the highest temperature. Therefore, outside the 8–12 μm atmospheric window region, the downwelling spectral radiation follows closely the respective blackbody radiation determined by the near-surface temperature for both scenarios and all crystal habits. Within the atmospheric window the downwelling spectral irradiance is less than the respective Planck-function because in this spectral region the gaseous atmospheric constituents do not absorb or emit much thermal IR radiation. The downwelling irradiance at the ground is nearly uninfluenced by the cirrus which is situated too high (i.e., too far away) to effectively impact the downwelling thermal IR spectral irradiance at the surface. Therefore there is also no shape dependence of the curves; the lines (representing cloudless and cloudy results) are indistinguishable from each other in this case.

[52] In general, the impact of the ice crystal shape on downwelling thermal IR spectral irradiance is in accordance with that for the broadband radiation (Figures 3b and 4b). The strongest effects are obvious in the vicinity of the cirrus. However, even though the relative impact seems high, the absolute influence of the particle habit is less than 2 W m^{-2} μm^{-1}, even at cirrus base and within the cirrus (not shown).

4.4.1.2. Upwelling Spectral Thermal IR Irradiance

[53] The upwelling thermal IR spectral irradiance at the Bottom of Atmosphere (BOA) is clearly determined by the thermal IR emission of the surface in correspondence with

the surface temperature and Planck's law (not shown). Needless to say, there are no effects of ice crystal shape for both scenarios (N = constant, IWC = constant) on the spectra of upwelling irradiance at the BOA emitted by the surface. At cirrus base (Figure 5d) the upwelling irradiance shows the combined effect of reduced surface emission (surface emission included in Figures 5d and 5c as pluses) and absorption/emission by the atmospheric gases beneath the cirrus. Within the atmospheric window wavelength region (about 8–12 μm) most of the surface-emitted irradiance reaches the cirrus base (except in the 9.6 μm O_3 absorption band). The reduction of the upwelling irradiance in the atmospheric window region is caused by the absorption due to continuum gas absorption (mainly H_2O). The corresponding emission takes place at higher, i.e., colder altitudes. However, the difference between the surface emission (pluses) and the upwelling irradiance in the atmospheric window (roughly 15%) seems quite high. This is due to the very large water vapor amount present in the subtropical environment of the CRYSTAL-FACE experiment. Additional simulations assuming an artificial reduction of the water vapor amount in the simulations drastically decreased the difference between the pluses and the upwelling irradiance in the atmospheric window spectral region (not shown here).

[54] The gas absorption band around 15 μm (CO_2) wavelength is so dominant that the upwelling irradiance in the center of the CO_2 absorption band is purely driven by the respective Planck-emission (i.e., by the corresponding temperature, asterisks). The same holds for the water vapor absorption around the 6.3 μm wavelength band and for CO_2 near 4.3 μm wavelength. The O_3 absorption near 9.6 μm wavelength beneath the cirrus is less strong; hence the dip in the curve at 9.6 μm is less pronounced. With regard to the impact of ice crystal habit, it is not surprising that there is no ice crystal shape effect of the upwelling irradiance below the cirrus for both scenarios. Furthermore, it is evident that the cloudless and cloudy upwelling irradiance at cirrus base coincide.

[55] At the cirrus top (15.4 km, see Figure 5c) the situation is different. The upwelling irradiance outside the strong gas absorption bands is absorbed by the cirrus which emits at lower temperature. Thus the level is decreased compared to the cloudless case. As usual, this reduction depends on the optical thickness of the cirrus and its temperature. For the first scenario (N = constant), assuming spherical ice crystal shapes reduces upwelling irradiance stronger than under the presumption of aggregates, in correspondence with the respective optical thickness (see Table 2). This is opposite to the results of the second scenario (IWC = constant); in this case the lines representing the different crystal habits are below those for spheres (solid thick line).

[56] The picture for the upwelling irradiance escaping the atmosphere at the Top of Atmosphere (TOA) (not shown) is not very different from that shown in Figure 5c, except that the strong O_3 concentrations and respective strong absorption in the ozone absorption wavelength band above the cirrus reduces the radiation around 9.3 μm even further.

4.4.2. Low (Warm) Cirrus of Large Optical Thickness: 23 July 2002

[57] The simulated spectra of downwelling and upwelling thermal IR irradiance for this cirrus case are plotted in Figure 6. Please note that in this case only the results for the second scenario (IWC = constant) are presented. The cirrus observed on 23 July 2002 was situated at lower altitudes (i.e., in a warmer environment). Furthermore, it was optically thicker compared to the cirrus on 26 July 2002. Both of these influences, but primarily the lower altitude, cause some modifications compared to Figure 5. At the cirrus top (Figure 6a) the level of downwelling irradiance is higher because of the higher temperature compared to Figure 5a. In addition to the emitted irradiance at the O_3 and CO_2 absorption bands, absorption/emission due to water vapor becomes already noticeable. However, once again, no shape dependence can be distinguished for the downwelling irradiance above the cirrus.

[58] At cirrus base (Figure 6b) the emission due to the cirrus becomes evident outside the major gas absorption bands. For spheres the emitted irradiance by the cirrus nearly follows the respective Planck-curve (for higher optical thickness the cirrus emissivity approaches unity). For aggregates some deviations from the Planck-curve are obvious in the atmospheric window region.

[59] The upwelling thermal IR spectral irradiance at cirrus base (Figure 6d) can be interpreted in a similar way as Figure 5d, although the dips in the spectrum at the gas absorption bands are less pronounced. This is because the temperature at cirrus base is higher. Therefore the absorption of the upwelling irradiance by the gases is weaker. At cirrus top (Figure 6c) again the reduction of upwelling irradiance outside the major gas absorption bands is visible (mainly in the atmospheric window region). However, the shape dependence is weaker compared to the higher, optically thin cirrus case, which is in accordance with the results for the broadband thermal IR irradiance.

[60] In summary, the impact of crystal habit on downwelling and upwelling thermal IR irradiance can safely be neglected for this cirrus case, regardless of the scenario which is assumed.

4.5. Radiative Forcing of Cirrus

[61] From the spectra of the thermal IR upwelling and downwelling irradiances, $F_\lambda^\uparrow$ and $F_\lambda^\downarrow$, the thermal IR radiative forcing (spectral and broadband) of the two cirrus cases was calculated. The thermal IR spectral radiative forcing $\triangle F_{TOA,\lambda}$ (in W m^{-2} μm^{-1}) of the cirrus at the Top of Atmosphere (TOA) was calculated by:

$$\triangle F_{TOA,\lambda} = \left[F_\lambda^\uparrow(TOA)\right]_{clear} - \left[F_\lambda^\uparrow(TOA)\right]_{cloudy}, \quad (1)$$

with index "*clear*" indicating cirrus-free conditions and the index "*cloudy*" for the case when cirrus was included in the calculations. In a similar way the spectral radiative forcing of the cirrus at the Bottom of Atmosphere (BOA), $\triangle F_{BOA,\lambda}$, was calculated by:

$$\triangle F_{BOA,\lambda} = \left[F_\lambda^\uparrow(BOA) - F_\lambda^\downarrow(BOA)\right]_{clear} - \left[F_\lambda^\uparrow(BOA) - F_\lambda^\downarrow(BOA)\right]_{cloudy}. \quad (2)$$

[62] By replacing the thermal IR spectral upwelling and downwelling irradiance at the TOA and BOA by the respective broadband thermal IR irradiance in equations

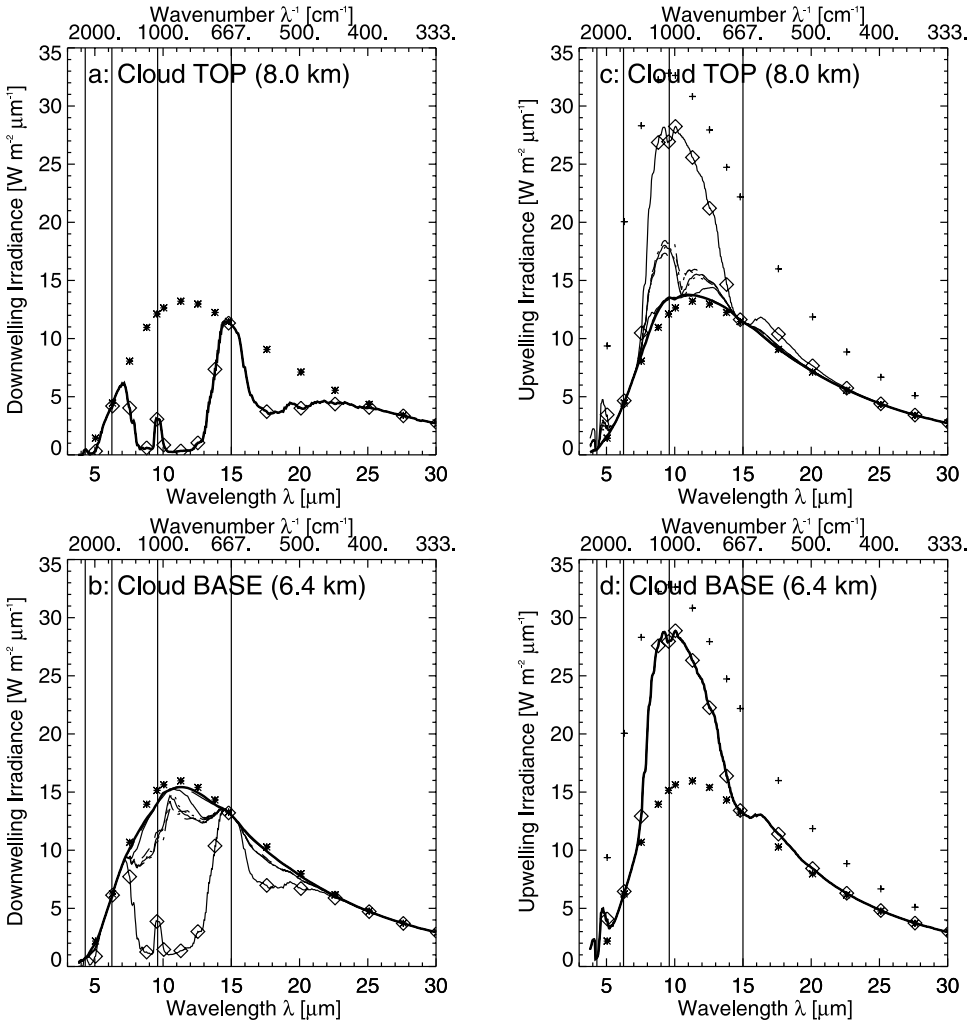

Figure 6. (a–d) Same as Figure 5 but for the low (warm) cirrus with large optical thickness observed on 23 July 2002.

(1) and (2), the broadband thermal IR cirrus radiative forcing, $\triangle F_{TOA}$ and $\triangle F_{BOA}$ (in W m^{-2}) of the cirrus at the TOA and BOA were derived.

[63] Additionally, from the sum of broadband solar (from W05) and broadband thermal IR radiative forcing the so-called broadband net radiative forcing $\triangle F_{TOA,net}$ and $\triangle F_{BOA,net}$ of the cirrus was derived. This was done for the first scenario only. Respective results are only briefly discussed in section 4.5.3, because a detailed discussion of the additional solar zenith dependence of the solar radiation would extend the paper beyond its focus, which is the thermal IR spectral range.

4.5.1. Spectral Thermal IR Radiative Forcing

[64] The spectral radiative forcing of the high (cold), optically thin cirrus is plotted in Figure 7. Figure 7a shows the result for the TOA (equation (1)), whereas Figure 7b presents the forcing at the BOA (equation (2)).

[65] Large effects of ice crystal shape are revealed in the atmospheric window region. Within the major gas absorption bands (vertical lines) the cirrus radiative forcing is close to zero, except for the O_3 absorption band at 9.6 μm wavelength. In accordance with the discussion above, for the first scenario (N = constant), at the TOA the strongest radiative forcing is exerted by the cirrus consisting of spherical ice crystals (thick solid line). For the second scenario (IWC = constant) spheres exhibit the least radiative forcing. The range of the radiative forcing covered by the different scenarios is quite remarkable, especially in the atmospheric window.

[66] At the BOA (Figure 7b) the radiative impact of the cirrus can be neglected over the entire thermal IR spectral range (mostly less than 1 W m^{-2} μm^{-1}). The cirrus is situated too high in the atmosphere to have any significant effect on the thermal IR radiation near the surface. This is in agreement with the discussion on Figures 3a and 3b, which has shown that there are only minor cirrus effects on upwelling and downwelling broadband thermal IR irradiance at the BOA.

[67] The respective results for the low cirrus of large optical thickness are presented in Figure 8. Similar spectral features as discussed for Figure 7 are seen for the 26 July 2002 case too. The cirrus on that day is situated in lower altitudes. Therefore the impact of this cirrus on the thermal IR spectral radiation field is smaller at the TOA and larger at the BOA which is in agreement with the broadband thermal IR irradiance shown in Figures 3c and 3d.

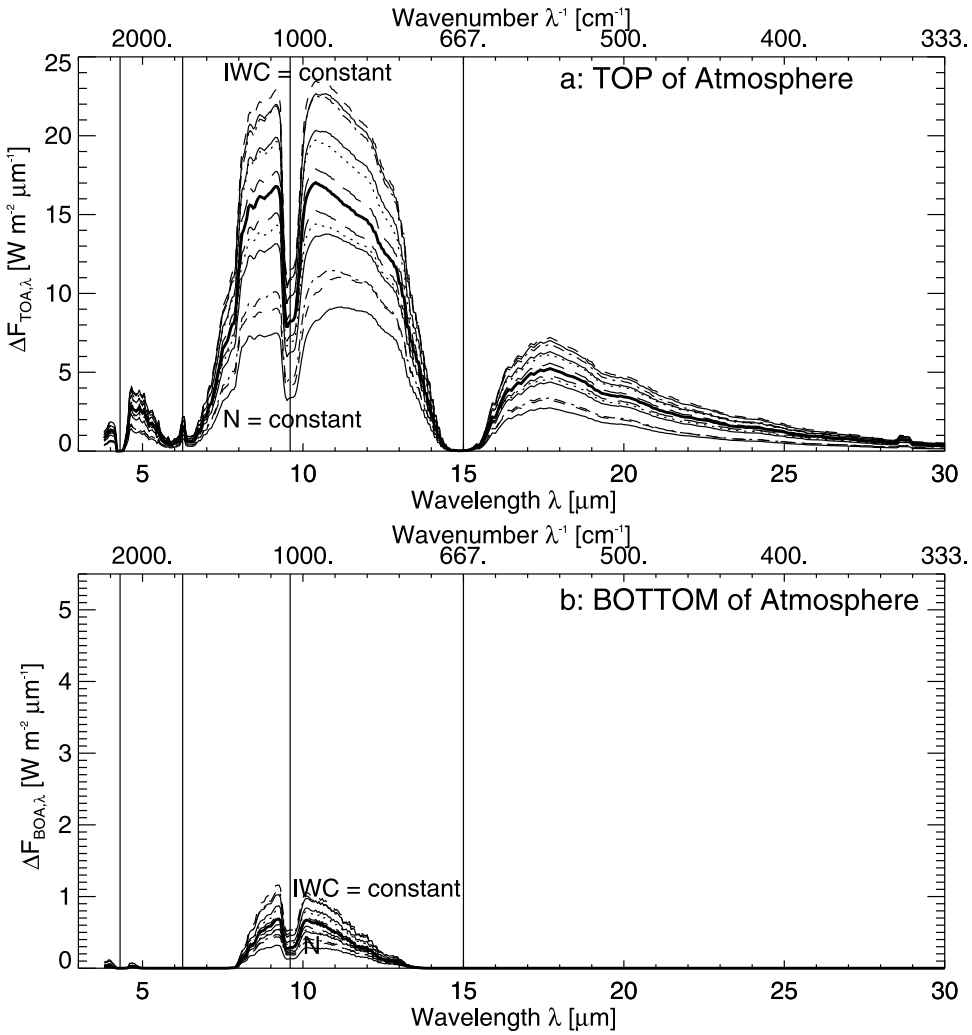

Figure 7. Spectral thermal IR radiative forcing of the high (cold), optically thin cirrus observed on 26 July 2002, simulated at (a) the top of atmosphere (TOA, see equation (1)) and (b) the bottom of the atmosphere (BOA, see equation (2)). The vertical lines mark the spectral location of the absorption bands of CO_2 [4.3 and 15 μm], H_2O [6.3 μm], and O_3 [9.6 μm]. The first scenario is labeled by *N* (or *N* = constant), and the second scenario is marked by *IWC* (or *IWC* = constant), respectively. For curve notation, see Table 1.

4.5.2. Broadband Thermal IR Radiative Forcing

[68] Table 3a (26 July 2002) and Table 3b (23 July 2002) contain the results for the two cirrus cases investigated. The values of the broadband thermal IR cirrus radiative forcing at the TOA are in accordance with Figure 3 (considering the difference between cloudy and cloudless upwelling irradiances at the TOA). At the TOA the thermal IR forcing of the cirrus is generally positive. Depending on the scenario chosen, the spherical crystal shape assumption leads to the largest radiative forcing due to the cirrus (first scenario; *N* = constant) or to lowest radiative forcing (second scenario; *IWC* = constant). The overall magnitude of the variation of the radiative forcing at the TOA of the high (cold) cirrus of small optical thickness (observed on 26 July 2002) is quite large (more than 100 W m^{-2}). In this cirrus case the shape of the ice crystals matters; the cirrus radiative forcing at the BOA is negligible.

[69] For the lower (warmer) cirrus with high optical thickness sampled on 23 July 2002 both, the absolute values and the effect of the habit of the ice crystals is much smaller at the TOA (see Table 3b) compared to Table 3a. As already discussed in section 4.3 the broadband thermal IR radiative forcing at the BOA is generally small, especially for the high cirrus observed on 26 July 2002.

4.5.3. Broadband Net Radiative Forcing

[70] The broadband net radiative forcing of cirrus is a function of the solar zenith angle θ_s because the solar radiative forcing is θ_s-dependent (see W05). As examples the broadband net radiative forcing for two values of θ_s (under which the data have been collected during CRYSTAL-FACE) are presented in Tables 4a and 4b. Only the first scenario (*N* = constant) is considered here.

[71] At the TOA and for the high, optically thin cirrus (Table 4a) mostly positive values of the broadband net radiative forcing are obtained, indicating a warming of the atmosphere due to the high cirrus (warming greenhouse effect dominating the cooling solar albedo effect). For low Sun ($\theta_s = 78°$) the broadband net radiative forcing is mostly

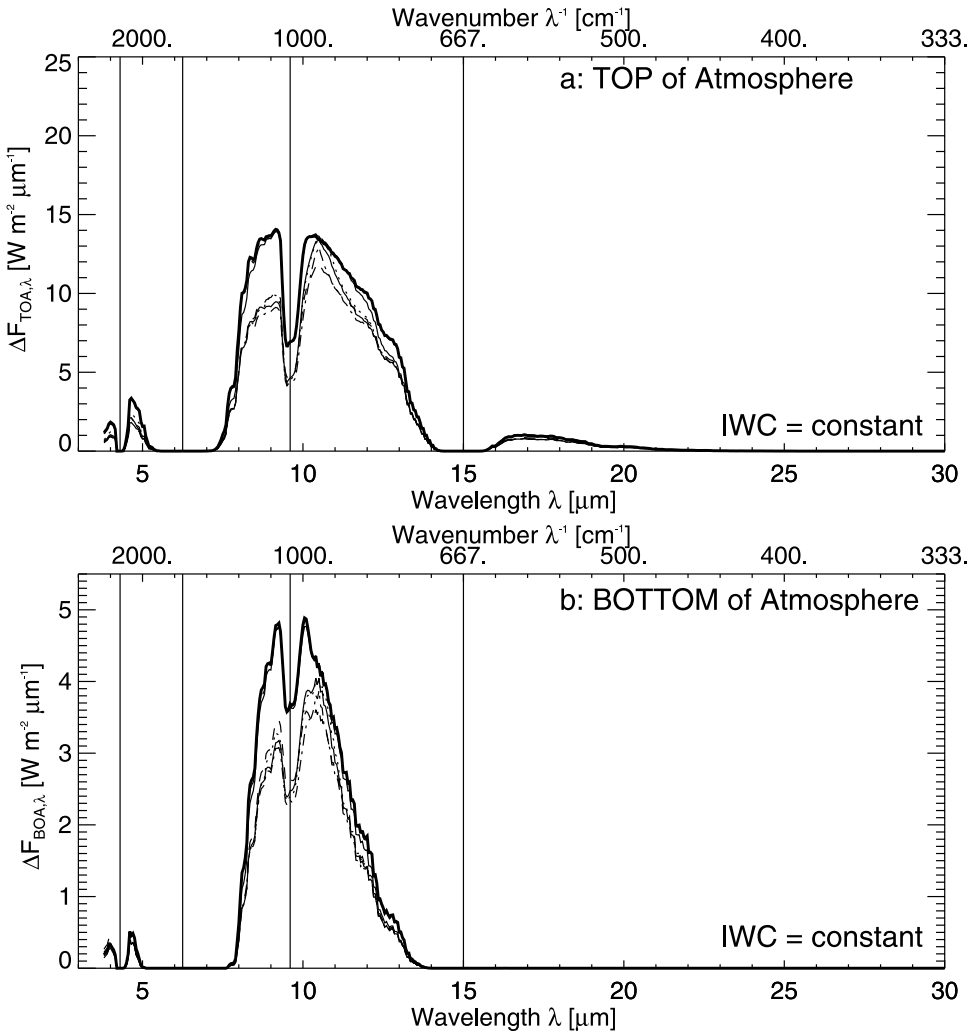

Figure 8. (a and b) Same as Figure 7 but for the low (warm) cirrus with large optical thickness observed on 23 July 2002.

lower compared to high Sun (θ_s = 21°). The assumptions about the shape of the ice crystals exert a considerable impact on the broadband net radiative forcing of the high, optically thin cirrus, and the forcing may even change its sign, thus changing the net radiative impact of the cirrus from warming (spheres) to slight cooling (aggregates). At the BOA this optically thin cirrus clearly cools with stronger cooling for high Sun (θ_s = 21°). At the BOA the net forcing is mainly driven by the solar radiative forcing (see for details W05).

[72] The lower cirrus of large optical thickness (23 July 2002, Table 3b) yields always a negative net radiative forcing and therefore cools both the entire atmosphere and the BOA. The cooling is strongest for high Sun, in this case

Table 3a. Broadband Thermal IR Radiative Forcing of the Cirrus Observed on 26 July 2002 (Optically Thin Cirrus) Calculated at the TOA ($\triangle F_{TOA}$) and BOA ($\triangle F_{BOA}$) and Assuming Different Ice Crystal Shapes[a]

	Top of Atmosphere: $\triangle F_{TOA}$		Bottom of Atmosphere: $\triangle F_{BOA}$	
Scenario (Constant =)	*N*	*IWC*	*N*	*IWC*
Sphere	124	124	2.0	2.0
Droxtal	112	131	1.8	2.1
Solid hexagonal column	107	146	1.6	2.4
Hollow hexagonal column	101	150	1.6	2.6
Hexagonal plate	79	163	1.4	3.1
Bullet rosette	75	173	1.3	3.4
Aggregate	63	167	1.0	3.1

[a]Two scenarios (*N* = constant and *IWC* = constant) are investigated. Unit is W m^{-2}.

Table 3b. Same as Table 3a but for the Cirrus Observed on 23 July 2002 (Cirrus of Large Optical Thickness)

	Top of Atmosphere: $\triangle F_{TOA}$		Bottom of Atmosphere: $\triangle F_{BOA}$	
Scenario (Constant =)	*N*	*IWC*	*N*	*IWC*
Sphere	64	64	15	15
Droxtal	65	64	15	15
Solid Hexagonal Column	64	51	15	12
Hollow Hexagonal Column	65	50	15	11
Hexagonal Plate	62	48	15	11
Bullet Rosette	60	50	14	11
Aggregate	50	61	11	14

Table 4a. Broadband Net Radiative Forcing of the Cirrus Observed on 26 July 2002 (Optically Thin Cirrus) Calculated at the TOA ($\triangle F_{TOA,net}$) and BOA ($\triangle F_{BOA,net}$) and Assuming Different Ice Crystal Shapes for the First Scenario (N = Constant)[a]

	Top of Atmosphere: $\triangle F_{TOA,net}$		Bottom of Atmosphere: $\triangle F_{BOA,net}$	
Solar Zenith Angle θ_s	78°	21°	78°	21°
Sphere	48	62	−51	−207
Solid hexagonal column	24	16	−55	−283
Hollow hexagonal column	20	20	−53	−273
Hexagonal plate	14	39	−44	−311
Bullet rosette	9.4	29	−47	−415
Aggregate	−5.2	11	−49	−435

[a]For the solar radiative forcing of the cirrus, see Table 3 in W05. Unit is W m^{-2}.

also the shape dependence of the broadband net radiative forcing appears to be strongest. For low Sun (θ_s = 78°) ice crystal shape does not significantly influence the broadband net radiative forcing of this cirrus.

5. Summary and Conclusions

[73] In this paper the effects of ice crystal habit on radiative properties and forcing of cirrus clouds in the thermal infrared (IR) wavelength range were investigated. Microphysical measurements (ice crystal number size distribution) from a field campaign (CRYSTAL-FACE) and a new library of optical properties of individual nonspherical ice crystals [*Yang et al.*, 2005] were combined to construct the input to a radiative transfer model. The model simulated the impact of ice crystal morphology on profiles of downwelling and upwelling (broadband and spectral) thermal IR irradiance, and the respective radiative forcing (spectral and broadband, thermal IR and net) of cirrus clouds.

[74] Two special cirrus clouds were studied in detail. On 26 July 2002 a high (13.1–15.4 km altitude), i.e., cold, cirrus was observed. The optical thickness of this cirrus was in the range of 1 (at 10.8 μm wavelength). This cloud was considered as optically thin cirrus case. The second cirrus was observed on 23 July 2002. It was located lower (6.4–8.0 km altitude); that is, this cirrus was embedded in a warmer atmosphere, and it had an optical thickness of about 7. This second case was referred to as an optically thick cirrus. The effects of both clouds on solar radiation were discussed previously in a companion paper [*Wendisch et al.*, 2005].

[75] A measurement-based modeling methodology was developed to systematically study the impact of crystal habit on thermal IR radiative properties and forcing of the two cirrus cases. Two scenarios have been investigated. First, the crystal number size distribution (and in consequence the number concentration N) of the ice crystals was kept constant when varying the crystal shape in the simulations. In this first scenario the ice water content (*IWC*) depends on crystal size, while N stays constant. In the second scenario the *IWC* was fixed in the simulations while N was allowed to vary.

[76] In the first scenario (fixed N) the impact of unknown crystal shape on the thermal IR radiative properties of the cirrus was computed on the basis of ice crystal number size distribution measurements alone, with no shape information at all. This approach led to a serious shape dependence of the resulting irradiances and cirrus radiative forcing for the high, optically thin cirrus case. For example, upwelling broadband thermal IR radiation above the high, optically thin cirrus might vary by 30% depending on the shape assumptions (≈65 W m^{-2}). The downwelling broadband thermal IR irradiance beneath this cirrus may even experience 70% changes due to ice crystal shape assumptions. However, it should be noted that the changes in terms of absolute values were comparably small in this case (≈25 W m^{-2}). The largest radiative impact of this cirrus, compared to the cloudless case, was exerted by assuming the spherical crystal shape. Least effects were simulated for the aggregate crystal habit. The reason is that spheres exhibit the largest total projected cross-sectional area if N is fixed, compared to any other assumed crystal habit. Thus it was concluded, that it is highly uncertain to simulate thermal IR radiative properties of high, optically thin cirrus on the basis of crystal number size distribution measurements alone, if no additional shape information is available. Ice crystal size distribution measurements in terms of ice crystal maximum length (leading to very different *IWC* and ice particle total projected cross-sectional area by assuming different ice particle shapes) are not suitable for use in radiation budget closure experiments.

[77] The second scenario (fixed *IWC*) showed opposite shape effects; that is, spheres exerted the least radiative effects, compared to all other crystal habits. That is because spheres had the least total projected cross-sectional area if *IWC* was kept constant. The shape effects on the radiative properties of the high, thin cirrus were of similar magnitude as in the first scenario, though the direction of the impact was opposite.

[78] With regard to spectral thermal IR irradiance it was shown that, similar to the broadband thermal IR irradiance, largest effects of ice crystal shape were observed for the high, optically thin cirrus. Similar to the results of the broadband thermal IR irradiance, the shape impact for the low, optically thin cirrus of large optical thickness could be neglected for the spectral thermal irradiance too. The strongest impact due to the ice crystal shape was found in the atmospheric window region (8–12 μm). Within the major gas absorption bands of CO_2 [4.3 and 15 μm], H_2O [6.3 μm], and O_3 [9.6 μm] the thermal IR radiation was completely insensitive to ice crystal shape.

[79] Similar conclusions were drawn for the thermal IR radiative forcing of the cirrus at the top of atmosphere

Table 4b. Same as Table 4a but for the Cirrus Observed on 23 July 2002 (Cirrus of Large Optical Thickness)

	Top of Atmosphere: $\triangle F_{TOA,net}$		Bottom of Atmosphere: $\triangle F_{BOA,net}$	
Solar Zenith Angle θ_s	78°	21°	78°	21°
Sphere	−24	−232	−57	−317
Solid hexagonal column	−31	−289	−59	−348
Hollow hexagonal column	−29	−262	−57	−321
Hexagonal plate	−22	−186	−50	−245
Bullet rosette	−24	−191	−49	−250
Aggregate	−32	−184	−51	−253

(TOA). Significant effects of ice crystal shape were observed for the high, optically thin cirrus. In the tropics thin cirrus is ubiquitous, so the impact of crystal habit may be very important here. One also should keep in mind that infrared works around the clock (24 hours), unlike solar that acts only part of the day. Spectrally, the largest effects of ice crystal habit were ascertained within the atmospheric window region; no shape impact was obvious within the gas absorption bands. The thermal IR (broadband and spectral) radiative forcing of the cirrus at the bottom of the atmosphere was low in general. Therefore no effects of ice crystal shape of the BOA thermal IR forcing were identified. The net radiative forcing of the cirrus showed most effects of ice crystal shape for high Sun in both cirrus cases.

[80] In general, for the low, optically thick cirrus case crystal habit did not seriously impact broadband and spectral thermal IR irradiances and the resulting forcing. This conclusion applied for both scenarios studied here (N = constant; IWC = constant). For the downwelling and upwelling broadband thermal IR irradiance in the second cirrus case (low altitude, large optical thickness) the impact of the shape assumptions was, on average, less than 15–20%. Thus for the low, optically thick cirrus the spherical shape assumption was appropriate to describe the thermal IR irradiances (broadband and spectral) above and below the cirrus as well as their radiative forcing.

[81] For the broadband thermal IR irradiances (downwelling and upwelling, below and above the cirrus) a comparison between measured and simulated values was conducted. A bias in upwelling thermal IR irradiance above the high, optically thin cirrus was observed. One possible source for the observed discrepancy between measured and simulated values was the neglect of effects due to horizontal inhomogeneities in the cirrus microphysical properties, that were not considered in the simulations. This bias was already discussed by *Fu et al.* [2000]. These authors also showed that for low, optically thick cirrus this bias should diminish, which was confirmed in our comparisons for the second cirrus case (low, optically thick cirrus observed on 23 July 2002). Otherwise acceptable agreement between measured and simulated broadband thermal IR was achieved except for the downwelling irradiance below the low, optically thick cirrus. The reason for the discrepancy in this case was mainly the poor colocation between the microphysical and radiation sampling of this cirrus, as already discussed by *Wendisch et al.* [2005].

[82] Finally we would like to emphasize that the maximum effects of ice crystal shape reported in this paper are upper boundaries of what might be expected in nature. The cirrus was considered in the simulations of this paper as consisting of ice crystals with uniform shape. In reality cirrus is most often composed of mixtures of ice crystals with different habits. Such a mixing leads to a systematic dampening of the maximum effects of ice crystal shape reported here. In the real atmosphere the effects of ice crystal shape will range in between the boundaries given in this paper.

[83] **Acknowledgments.** We are grateful to Warren Gore, Larry Pezzolo and Tony Trias from NASA Ames Research Center and John Pommier and Steve Howard from the Bay Area Environmental Research Institute for their engineering, computer and technical support during CRYSTAL-FACE. Darrel Baumgardner, Andy Heymsfield and Carl Schmitt have kindly provided their ice crystal size distribution data from CRYSTAL-FACE. Bernhard Mayer helped in the radiative transfer simulations. Ping Yang acknowledges support from U.S. National Science Foundation (ATM-0239605). We also wish to thank the NASA Earth Science Enterprise Radiation Science Program for supporting this research.

References

Baran, A. J. (2004), On the scattering and absorption properties of cirrus cloud, *J. Quant. Spectrosc. Radiat. Transfer*, *89*, 17–36.

Baran, A. J. (2005), The dependence of cirrus infrared radiative properties on ice crystal geometry and shape of the size-distribution, *Q. J. R. Meteorol. Soc.*, *131*, 1129–1142.

Baran, A. J., and P. N. Francis (2004), On the radiative properties of cirrus cloud at solar and thermal wavelengths: A test of model consistency using high-resolution airborne radiance measurements, *Q. J. R. Meteorol. Soc.*, *130*, 763–778.

Baran, A. J., S. J. Brown, J. S. Foot, and D. L. Mitchell (1999), Retrieval of tropical cirrus thermal optical depth, crystal size, and shape using a dual-view instrument at 3.7 and 10.8 μm, *J. Atmos. Sci.*, *56*, 110–592.

Francis, P. N., J. S. Foot, and A. J. Baran (1999), Aircraft measurements of the solar and infrared radiative properties of cirrus and their dependence on ice crystal shape, *J. Geophys. Res.*, *104*, 31,685–31,696.

Fu, Q., and K. Liou (1992), On the correlated k-distribution method for radiative transfer in nonhomogeneous atmospheres, *J. Atmos. Sci.*, *49*, 2139–2156.

Fu, Q., P. Yang, and W. B. Sun (1998), An accurate parameterization of the infrared radiative properties of cirrus clouds for climate models, *J. Clim.*, *25*, 2223–2237.

Fu, Q., W. B. Sun, and P. Yang (1999), Modeling of scattering and absorption by nonspherical cirrus ice particles at thermal infrared wavelengths, *J. Atmos. Sci.*, *56*, 2937–2947.

Fu, Q., B. Carlin, and G. Mace (2000), Cirrus horizontal inhomogeneity and OLR bias, *Geophys. Res. Lett.*, *27*, 3341–3344.

Jenson, E., D. Starr, and O. B. Toon (2004), Mission investigates tropical cirrus clouds, *Eos Trans. AGU*, *85*(5), 45.

Liou, K.-N. (1986), Influence of cirrus clouds on weather and climate processes: A global perspective, *Mon. Weather Rev.*, *114*, 1167–1199.

Lynch, D. K., , K. Sassen, D. O. Starr, and G. Stephens (Eds.) (2002), *Cirrus*, Oxford Univ. Press, New York.

Macke, A., P. N. Francis, G. M. McFarquhar, and S. Kinne (1998), The role of ice particle shapes and size distributions in the single scattering properties of cirrus clouds, *J. Atmos. Sci.*, *55*, 2874–2883.

Mayer, B., and A. Kylling (2005), Technical note: The libRadtran software package for radiative transfer calculations—Description and examples of use, *Atmos. Chem. Phys.*, *5*, 1855–1877.

McFarquhar, G. M., and A. J. Heymsfield (1997), Parameterization of tropical cirrus ice crystal size distributions and implications for radiative transfer: Results from CEPEX, *J. Atmos. Sci.*, *54*, 2187–2200.

McFarquhar, G. M., P. Yang, A. Macke, and A. J. Baran (2002), A new parameterization of single scattering solar radiative properties for tropical anvils using observed ice crystal size and shape distributions, *J. Atmos. Sci.*, *59*, 2458–2478.

Mishchenko, M. I., J. W. Hovenier, and L. D. Travis (Eds.) (2000), *Light Scattering by Nonspherical Particles*, Elsevier, New York.

Mitchell, D. L., and W. P. Arnott (1994), A model predicting the evolution of ice particle size spectra and radiative properties of cirrus clouds. Part II: Dependence of absorption and extinction on ice crystal morphology, *J. Atmos. Sci.*, *51*, 817–832.

Mitchell, D. L., A. Macke, and Y. Liu (1996), Modeling cirrus clouds. Part II: Treatment of radiative properties, *J. Atmos. Sci.*, *53*, 2967–2988.

Rädel, G., C. J. Stubenrauch, R. Holz, and D. L. Mitchell (2003), Retrieval of effective ice crystal size in the infrared: Sensitivity study and global measurements from TIROS-N Operational Vertical Sounder, *J. Geophys. Res.*, *108*(D9), 4281, doi:10.1029/2002JD002801.

Ricchiazzi, P., S. Yang, C. Gautier, and D. Sowle (1998), A research and teaching software tool for plane-parallel radiative transfer in the Earth's atmosphere, *Bull. Am. Meteorol. Soc.*, *79*, 2101–2114.

Schlimme, I., A. Macke, and J. Reichardt (2005), The impact of ice crystal shapes, size distributions and spatial structures of cirrus clouds on solar radiative fluxes, *J. Atmos. Sci.*, *62*, 2274–2283.

Stamnes, K., S. C. Tsay, W. Wiscombe, and K. Jayaweera (1988), A numerically stable algorithm for discrete-ordinate-method radiative transfer in multiple scattering and emitting layered media, *Appl. Opt.*, *27*, 2502–2509.

Stubenrauch, C. J., R. Holz, A. Chédin, D. L. Mitchell, and A. J. Baran (1999), Retrieval of cirrus ice crystal sizes from 8.3 and 11.1 μm

emissivities determined by the improved initialization inversion of TIROS-N Operational Vertical Sounder observations, *J. Geophys. Res.*, *104*(D24), 31,793–31,808.

Wendisch, M., P. Pilewskie, J. Pommier, S. Howard, P. Yang, A. J. Heymsfield, C. G. Schmitt, D. Baumgardner, and B. Mayer (2005), Impact of cirrus crystal shape on solar spectral irradiance: A case study for subtropical cirrus, *J. Geophys. Res.*, *110*, D03202, doi:10.1029/2004JD005294.

Yang, P., B.-C. Gao, B. A. Baum, Y. X. Hu, W. J. Wiscombe, S.-C. Tsay, D. M. Winker, and S. L. Nasirie (2001), Radiative properties of cirrus clouds in the infrared (8–13 μm) spectral region, *J. Quant. Spectrosc. Radiat. Transfer*, *70*, 473–504.

Yang, P., H. Wei, H. Huang, B. A. Baum, Y. X. Hu, G. W. Kattawar, M. I. Mishchenko, and Q. Fu (2005), Scattering and absorption property database for nonspherical ice particles in the near- through far-infrared spectral region, *Appl. Opt.*, *44*, 5512–5523.

Zhang, Y., A. Macke, and F. Albers (1999), Effect of crystal size spectrum and crystal shape on stratiform cirrus radiative forcing, *Atmos. Res.*, *52*, 59–75.

P. Pilewskie, Laboratory for Atmospheric and Space Physics, Department of Atmospheric and Oceanic Sciences, Duane Physics, Room D-317, Campus Box 311, University of Colorado, Boulder, CO 80309-0392, USA. (peter.pilewskie@lasp.colorado.edu)

M. Wendisch, Institute for Atmospheric Physics, Johannes Gutenberg-University, Becherweg 21, D-55099 Mainz, Germany. (wendisch@uni-mainz.de)

P. Yang, Department of Atmospheric Sciences, Texas A&M University, TAMU 3150, College Station, TX 77843, USA. (pyang@ariel.met.tamu.edu)